

The supplementary figures show the data for three Ti phosphate ALD processes, while similar data is available for Al, Zn and Sn phosphates.

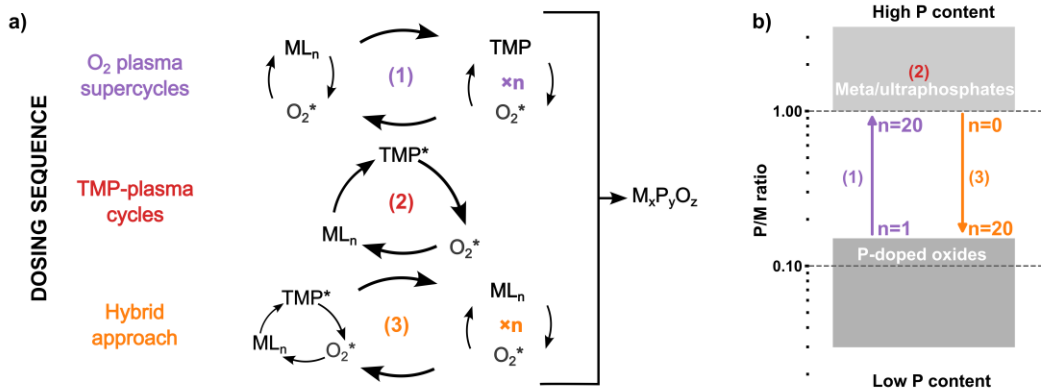


Figure 1. (a) Different dosing schemes studied during this work, and (b) schematic representation of stoichiometry control achievable using these approaches. Note that the P/M ratio is presented on a logarithmic scale.

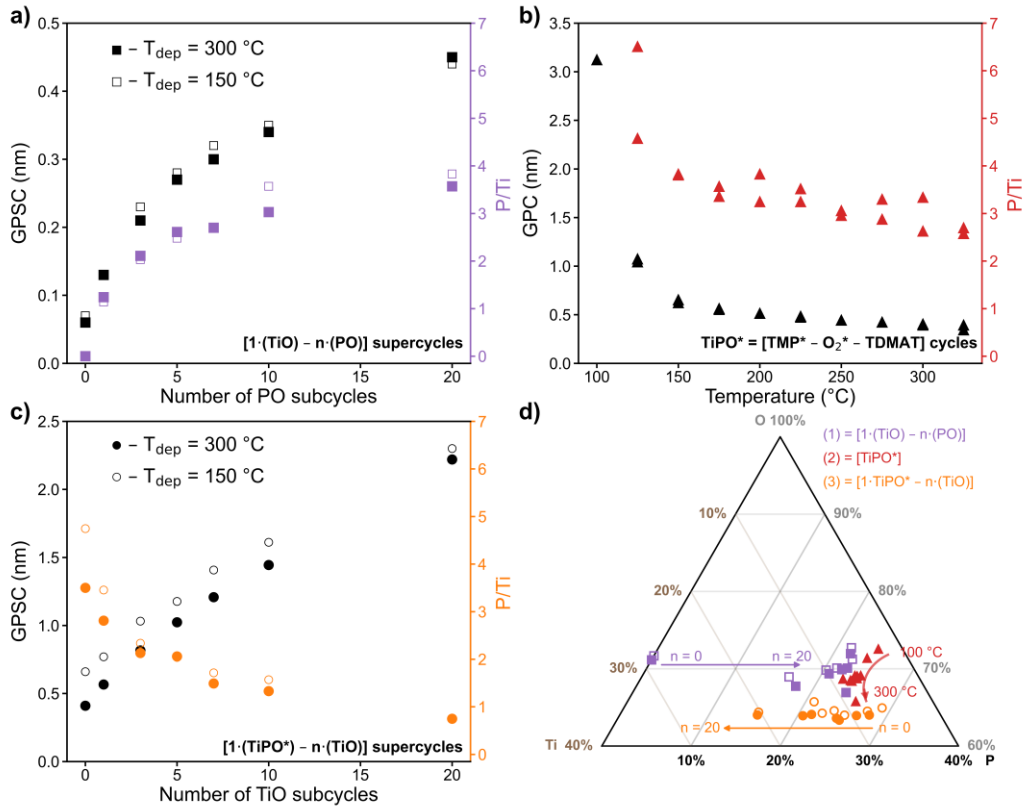


Figure 2 (a) Growth and compositional characteristics for $[1 \cdot (MO) - n \cdot (PO)]$ supercycles for $M = Ti$ that demonstrate increasing P incorporation with n , from P-doped metal oxide to meta/pyrophosphate films. (b) Growth and compositional characteristics for TMP plasma-based MPO (MPO*) films for $M = Ti$, deposited using $[TMP^* - O_2^* - TDMAT]$ cycles, which demonstrate increasing P incorporation with decreasing T_{dep} , and yield highly P-rich meta/ultraphosphate films at all tested T_{dep} . (c) Growth and compositional characteristics for supercycles combining ALD cycles of TMP plasma-based MPO (MPO*) and MO $[1 \cdot MPO^* - n \cdot (MO)]$ (for $M = Ti$), and which demonstrate a reduction in P incorporation from meta/ultraphosphate to P-doped metal oxide films, with increasing n . (d) Ternary phase diagram representation of control over film stoichiometry afforded by the approaches described in this work. It should be noted that the axes in the diagram denote atomic fractions of Ti, O and P, calculated from elemental composition, measured by XPS.

Full forms: ML_n = metal precursor; O_2^* = O_2 plasma; TMP^* = plasma polymerised TMP; MO = metal oxide; PO = phosphorus oxide; T_{dep} = deposition temperature